Pergamon

0094-5765(95)00111-5

Acta Astronautica Vol. 36, No. 6, pp. 337–346, 1995

0094-5765/95 $9.50 + 0.00

NEO INTERACTION WITH NUCLEAR RADIATION

PETER HAMMERLING and JOHN L. REMO
Quantametrics Inc., 1 Brackenwood Path, Head of the Harbor, St James, NY 11780, U.S.A.

(Received 3 November 1994; revised version received 6 September 1995)

Abstract—This paper investigates one of several possible means of deflection of a large near-Earth object (NEO) on a potential collision course with Earth by means of modest velocity changes ($\Delta V \approx 1$–200 cm/s) applied to the NEO at perihelion. Given the present uncertainty in the geometry, topography and materials properties of the asteroids and/or comets, a deflection mechanism is required which is relatively insensitive to such details. Stand-off nuclear devices present an option to fulfill this criterion. Momentum can be transferred by several mechanisms: directly by means of the kinetic energy of the debris or, more efficiently, by ablation resulting from the absorption of X-rays. Thermonuclear devices additionally produce high energy neutrons. Using approximate models of the various types of NEO materials and tabulations from the literature, we construct effective X-ray and neutron mass absorption coefficients. The latter are incorporated into a simple model to calculate the impulse, and hence the velocity change imparted by the various nuclear products to all the NEO materials models.

1. INTRODUCTION

Ever since 1932 when Reinmuth discovered 1862 Apollo, the first Earth-crossing asteroid (ECA), it has been understood that the Earth's orbit resides within a swarm of asteroids and comets. It was also realized that the orbits of these Earth-crossing asteroids and comets (ECCs) can be perturbed to intersect and even impact the Earth's surface. In 1971, Gehrels discovered Daedalus upon initiating a systematic wide field search for ECAs. Soon after, other asteroid surveys were also initiated resulting in the discovery of numerous ECAs and ECCs. An ECA is defined [1,2] as an object moving on a trajectory capable of intersecting the Earth's capture cross-section as a result of on-going (on the order of tens of thousands of years) long-range gravitational perturbations due to the Earth and other planets. ECCs may be defined in an analogous way. These surveys found that about 90% of the potential Earth-crossing (and impacting) objects are considered to be near-Earth asteroids or short-period comets, with the remaining 10% intermediate or long-period comets having orbital periods longer than 20 years. As a group these bodies are called NEOs (near-Earth objects), which can be classified as having orbits that closely approach and possibly intersect the Earth's orbit (~ 1 AU).

A model of the true population of ECAs tested against observed discoveries made during searches at the Palomar 46-cm Schmidt telescope and the University of Arizona Spacewatch telescope [3] indicates that there are about 20 ECAs larger than 5 km in diameter, about 1500 larger than 1 km in diameter and 135,000 larger than 100 m in diameter. There are also thought to be an order of magnitude greater number of smaller NEOs that have not yet been detected [2,4]. While none of the approx. 1700 suspected ECAs larger than 1 km in diameter currently presents a hazard, they are nonetheless capable of developing Earth-impacting trajectories over a period of thousands of years. This population model does not take into account the direct hazards from ECCs, many of which are extremely difficult to detect. These numbers present but part of the potential hazard, an additional source of Earth orbit-crossing objects can arise from debris resulting from tidal break-up (Roche lobe) of both long- and short-period comets in Sun-grazing orbits [5]. This latter class of NEOs can present a hazard if the debris stream intersects the Earth's orbit at one of its nodes. The potential danger to the Earth from comets which undergo chaotic orbital variations represents another facet of the NEO hazard whose statistics have yet to be understood.

Despite the fact that NEOs were regarded to have collided with the Earth throughout its history, up to about 1980 there had been little concern about the likelihood of a terrestrial collision with an ECA or ECC. However, interest in ECAs and ECCs was stimulated largely as an outgrowth of the work of Alvarez *et al.* [6], which in 1980 proposed that an asteroid or comet impacted with the Earth and initiated a global disturbance that resulted in the mass extinction of the dinosaurs as well as other life-forms over a broad range of genera and species.

The recent impact of comet Shoemaker–Levy 9 (SL-9) on Jupiter has underscored the fact that near-Earth objects not only cross planetary orbits,

but can also impact them with devastating consequences [7]. The SL-9 event dramatically presented the possible hazards from NEOs in a context hitherto regarded as unlikely. To this end it is prudent to consider analytical models which address orbit management as a means of protecting the Earth against a direct NEO threat.

2. DEFLECTION OF LARGE ASTEROIDS

This paper addresses one method of deflecting large asteroids on a collision course with the Earth. For example, an asteroid of around 20 m in diameter has the potential destructive capacity of over 1000 MT of TNT. Such a possibility, though remote, is not inconceivable, and has been the topic of several recent conferences [8–13] and articles [14–17]. Given sufficient warning, a mission could be launched to apply a velocity change (ΔV) to the asteroid in question so as to cause it to miss the Earth. Ideally, a first-order estimate of the precise value of the velocity change depends on the asteroid's orbit, where in the orbit the impulse is applied and the desired miss distance. For a miss distance of 10,000 km and interception at perihelion, ΔVs for typical, known asteroids range from around a centimeter per second to several meters per second [8, 18]. The question then, is how best to apply the required impulse? This is a function of many parameters which include the mission economics and logistics, the technical means deemed most appropriate and the materials properties of the NEO. Subsurface momentum coupling from conventional (HE) and nuclear (NE) explosives has been discussed by Remo and Sforza [19], while a more general review of the momentum coupling options (pulsed laser, kinetic energy impactors, NE and HE explosives) can be found in the paper of Shafer *et al.* [20]. The mechanism that appears to be the least sensitive to current uncertainties in composition and shape, i.e. to the geology and materials properties of asteroids, is a stand-off nuclear burst [21,22]. Since the latter irradiates approximately half the surface area, it is also less liable initially to add additional angular momentum to the asteroid as would be the case for a misplaced surface burst, penetration device or thruster. It can be shown that for the ratio of the rotational, T, to the kinetic energy, E, to be small, that $T/E = (V_A/\Delta V)^2 \ll 1$; $V_A \equiv \omega[\Lambda]$ where ω is the angular velocity and Λ a characteristic length.

A simple model [22–25] adapted to treat stand-off momentum transfer is discussed in more detail than previously [22] and is then applied to specific classes of asteroid analog materials, meteorites. This model is not meant to take the place of more detailed calculations. However, the latter require multi-group neutron and radiation transport and equation of state data coupled to a full hydrodynamic code in order to estimate the energy deposition and impulse given to the asteroid. Since accurate models for asteroids and materials' properties are lacking for the latter, it is felt that a first-order approach is preferable at this time.

The energy liberated in a nuclear explosion in space can be divided into that coming directly from the nuclear reactions and that from the heated case and weapon material. Table 1, from the ICARUS report [26] and based on the information in Glasstone [27], gives the fractional distributions of the energy. Based on the nuclear reaction kinetics, Glasstone's table applies to fission devices, although this is not explicitly stated. The prompt gamma-rays are emitted in the first instants of the explosion, the delayed gamma and beta radiation come from the fission products. The bulk of the radiation is emitted in thermal X-rays. For a thermonuclear device the energy release derives approximately equally from fission and fusion [27]; most of the fusion energy is in the form of high-energy neutrons. The neutrons are slowed down by collisions with the fuel and case and can cause fast fission reactions. This gives rise to a spectrum of energy values of the surviving neutrons which is not given. Below we estimate the impulse given to the asteroid by the various sources listed in Table 1: the debris, and ablation due to the absorption of gamma-rays, X-rays and neutrons. The results are also presented in graphical form in the figures for representative values of the opacities.

3. IMPULSE DUE TO DEBRIS

The specific impulse from the debris is approximately:

$$I_D = \frac{M_D}{4\Pi L^2} \langle V_D^2 \rangle^{1/2} \tag{1}$$

where M_D is the debris mass, L the distance from the

Table 1(a). Fractional energy distribution (fission device) [26,27]

Nuclear radiation		Thermal radiation	
Prompt gamma-ray	0.001	X-rays	0.70
Neutrons	0.01	u.v., visible, i.r.	0.05
Delayed gamma-rays	0.02	Debris, kinetic energy	0.20
Delayed beta-rays	0.02		

Table 1(b). Fractional energy distribution used for the fusion device

Source	X-rays	Neutrons	Gamma-rays	Debris	Other
Fraction	0.55	0.20	0.01	0.20	0.04

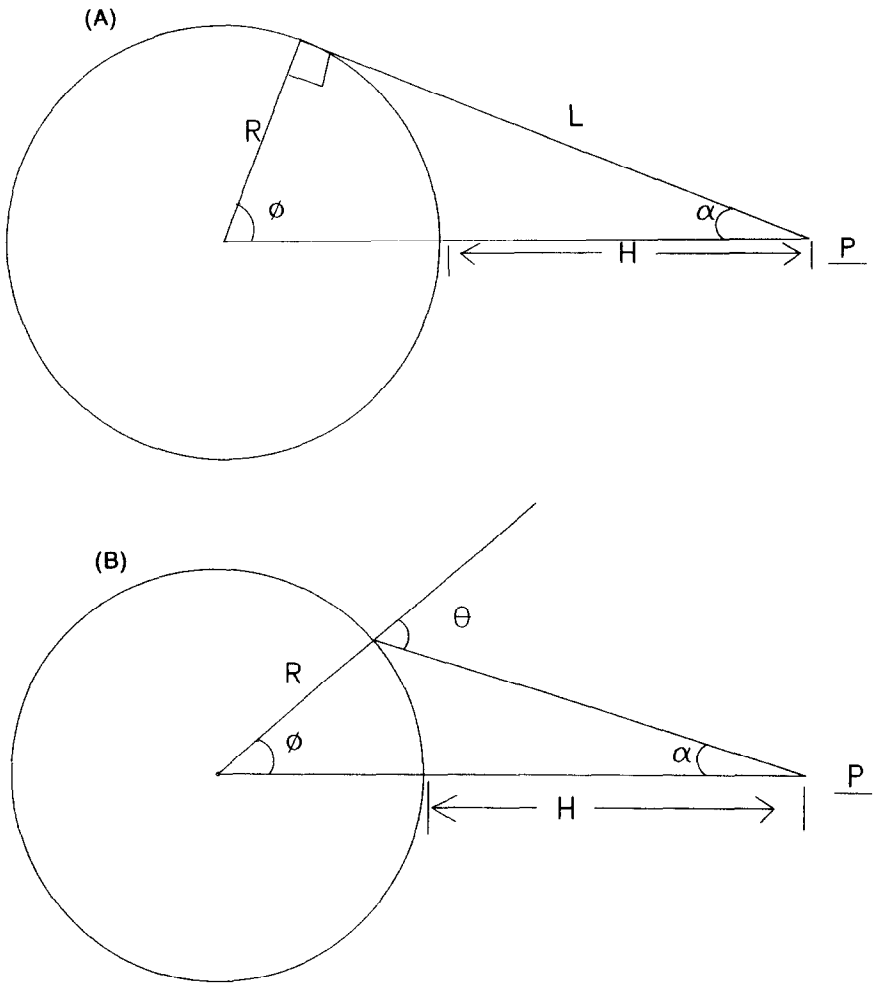

Fig. 1. Encounter geometry. (a) The burst is assumed to occur at point P at a stand-off distance H from a spherical NEO of radius R. (b) For angles (α, ϕ) less than their maximum values shown in (A), a typical ray has an angle of incidence θ with respect to the normal to the sphere. With $\chi \equiv H/R$, $\sin\theta = (1+\chi)\sin\alpha$.

burst to the asteroid and $\langle V_D^2\rangle^{1/2}$ is the RMS velocity of the debris. Here and in what follows we assume that the distance from the burst is much larger than the size of the object. The RMS velocity is related to the energy in the debris, E_D, by:

$$\tfrac{1}{2}M_D\langle V_D^2\rangle = E_D = \eta Y \tag{2}$$

where Y is the total yield and η the fraction of the yield appearing in the debris. The specific impulse also is given by:

$$I_D = (M_A/A)\Delta V_D \tag{3}$$

where M_A is the asteroid's mass and A its (total) area. The velocity change is, on combining eqns (1)–(3), and taking $\eta = 0.2$:

$$\Delta V_D = (A/M_A)\frac{\sqrt{2(0.2)M_D Y}}{4\Pi L^2}$$

$$= \frac{4.1\times 10^9}{M_A}\Delta\Omega\sqrt{M_D Y(\mathrm{MT})}\ \mathrm{cm/s}. \tag{4}$$

In the last term of the right hand side of the above expression the yield is in MT(TNT equivalent) and the mass is in kg.

The geometry of the encounter is shown in Fig. 1. The fractional solid angle, $\Delta\Omega \equiv (A/4\Pi L^2)$, depends on the ratio, $\chi = H/R$, of the stand-off distance, H, to the radius, R, for a spherical asteroid, and L corresponds to the tangential distance in Fig. 1.

With reference to Fig. 1, the fraction of the area irradiated is $f = 1/2[1-\cos\phi = \chi/(1+\chi)]$, and $\Delta\Omega = f/[\chi^2 + 2\chi]$. Similarly, the fraction of the energy liberated and subtended by the NEO is $g = 1/2[1-\sin\phi = (\chi^2+2\chi)^{1/2}/(1+\chi)]$. There is thus a trade-off between a more uniform irradiation and the energy requirements. For example, for $\chi = 2$, $f = 1/3$ and $\Delta\Omega = 1/24$. The value, $\chi = \sqrt{2}-1$, $(\chi = 0.414)$ for which $f = 0.15 = \Delta\Omega$ and, in Fig. 1, $\varphi = \alpha = 45°$, results from requiring $f+g$ be a maximum (see also [18]). Finally, Hyde [21], using a simple model, found, upon numerical integration, that $\chi = 0.5$ close to the above geometric optimum.

Taking $M_D = 300$ kg [23],

$$\Delta V_D = \frac{7.1 \times 10^{10}}{M_A} \Delta\Omega \sqrt{Y(\mathrm{MT})} \text{ cm/s.} \quad (5)$$

Since the mass of a kilometer size asteroid can exceed 10^{12} kg, the debris contribution can be neglected on this scale. The debris can be effective for objects of the order of 200 m diameter for the parameters used in this example. The effectiveness of the debris in deflecting large diameter objects could be enhanced if the mass of the debris and hence the coupling to it were increased. For yields in excess of 1 MT, the mass of the debris presumably increases, assuming it is scaled according to $M_D \sim Y^{2/3}$ the velocity increment is enhanced over that in eqn (5) only by $\Delta V_D \propto Y^{1/3}$.

4. IMPULSE ANALYSIS FOR RADIATION

We first describe the analytical model used to estimate the impulse [22].

The specific impulse (momentum per unit area), I, imparted by ablation due to X-ray or neutron absorption is found by integrating the differential relationship:

$$dI = \rho V \, dx \quad (6)$$

where

$$V^2/2 = \epsilon(x) - \epsilon_v \quad (7)$$

ρ is the density, $\epsilon(x)$ and ϵ_v are the incident energy per unit mass and vaporization energy per unit mass, respectively, and dx is the radial differential to the NEO surface. $\epsilon(x)$ is related to the absorbed fluence F, and the opacity μ (cm^2/g), by

$$\epsilon = \mu F. \quad (8)$$

Therefore

$$I = \sqrt{2} \int_0^{X_v} (\mu F - \epsilon_v)^{1/2} \rho \, dx \quad (9)$$

where X_v is the evaporation depth.

Additionally, it is assumed that the fluence varies with the penetration depth according to

$$F = F_0 \exp(-\rho\mu x/\cos\vartheta) \quad (10)$$

where ϑ is the angle between the incident radiation and the normal to the surface. Assuming a nuclear device explodes at a distance L from the NEO's surface, the incident fluence is,

$$F_0 = \eta Y/4\pi L^2$$
$$= 1.33 \times 10^5 \eta Y(\mathrm{MT}) \Delta\Omega/D^2 \text{ J/cm}^2 \quad (11)$$

where the yield, Y, is expressed in MT (TNT equivalent) and D, the asteroid diameter, in km. η denotes the fraction of the yield in X-rays, neutrons or gamma-rays. The temperature variation of the opacity is ignored. For simplicity the obliquity factor, $\cos\vartheta$, is set equal to unity which is valid for not too large values of the angle α of Fig. 1. For example, using $\chi = 0.414$ and $\alpha = 22.5°$, instead of its maximum value, $1/\cos\vartheta = 1.01$.

The specific impulse can be easily obtained by using the scaled, non-dimensional, variables

$$I = (\sqrt{\epsilon_v}/\mu) I^*$$
$$F_0^* = F_0/F_{\min} \geqslant 1$$
$$F_{\min} = \epsilon_v/\mu. \quad (12)$$

$F_{\min}$ represents the minimum fluence that is required to evaporate the material.

The evaporation depth is given by:

$$X_v = (\cos\vartheta/\rho\mu) \ln F_0^*. \quad (13)$$

With this form, the integral can be readily evaluated

$$I^* = 2\sqrt{2}\{\sqrt{F_0^* - 1} - \tan^{-1}[\sqrt{F_0^* - 1}]\}. \quad (14)$$

Note that the material properties in this model are entirely contained in the simple ratios of eqn (12).

If, instead of an exponentially decreasing absorption, one used a constant absorption model up to X_v and zero thereafter, the above calculation gives

$$I^* = \sqrt{2(F_0^* - 1)}. \quad (15)$$

These and other similar models also have been discussed by Lawrence [24,25]. In the asymptotic regime, $F_0^* \gg 1$, and, using eqn (12)

$$I = 2\sqrt{2F_0/\mu} \quad \text{exponential absorption} \quad (16a)$$
$$= \sqrt{2F_0/\mu} \quad \text{constant absorption} \quad (16b)$$

ϵ_v, does not appear in the expressions in this limit, but of course must be taken into account in determining if indeed $F_0^* \gg 1$. I is usually measured in taps (g/cm-s).

It is seen that in the asymptotic limit, other than the fact the specific impulse for exponential absorption is twice that for constant absorption, there is the same parametric dependence on the fluence and the opacity in eqns (16a) and (16b). The surface materials properties of the asteroid are expressed through μ. The fundamental assumptions of the model are mono-dimensionality, absorption coefficients independent of depth (i.e. uniformity of composition) and temperature, and neglect of viscosity and thermal conduction.

Hence, for a given yield, energies of vaporization and the mass absorption coefficients, the impulse can be calculated from eqns (12) and (14). The resulting velocity change of the asteroid can be obtained from the relation,

$$I = m\Delta V \quad (17)$$

where m is the areal mass density of the asteroid. In terms of Öpik's [28] shape parameter, B, and the mass density, ρ,

$$m = \rho R/B. \quad (18)$$

($B = 3$ for a sphere.)

Finally, we have

$$\Delta V = (2\sqrt{2}/m\mu)\sqrt{\epsilon_v}\{\sqrt{F_0^* - 1} - \tan^{-1}[\sqrt{F_0^* - 1}]\}. \quad (19)$$

In terms of the non-dimensional quantities,

$$\Delta V^* \equiv \Delta V/\sqrt{\epsilon_v} \quad \text{and} \quad m^* \equiv m\mu, \quad (20)$$

we have,

$$\Delta V^* = (2\sqrt{2}/m^*)\{\sqrt{F_0^* - 1} - \tan^{-1}[\sqrt{F_0^* - 1}]\}. \quad (21)$$

As discussed in the APS report [23] and by Lawrence [24], a useful way of contrasting experimental data with theory is to plot the impulse coupling coefficient,

$$C_m = I/F_0 \quad (22)$$

versus the incident fluence, F_0. The units of C_m are conventionally taken to be dyne-s/J. The impulse coupling coefficient has long been used extensively to analyze laser-induced impulse [24,29] but is not restricted to that application. In terms of the non-dimensional quantities defined above,

$$C_m^* = I^*/F_0^*$$
$$\Delta V^* = (F_0^*/m^*)C_m^*$$
$$C_m^* = \sqrt{\epsilon_v}\, C_m. \quad (23)$$

When I^* is given by eqn (14), C_m^* is maximal for $F_0^* = 6.434$, when $C_m^* = 0.5124$ [24]. For the problem under discussion, as will be seen below, for many of the values of the parameters, C_m^* is not optimal in this sense.

In the next sections we discuss the contributions to the opacities due to gamma-rays, X-rays and neutrons. Although they are not an important contributor for our purposes, we include the gamma-ray contribution for completeness.

5. OPACITIES

5.1. Gamma-ray

According to Glasstone [27], the gamma-ray spectrum from a burst in outer space arises primarily from the delayed gammas produced by the fission products, the prompt gammas being absorbed in the case and nuclear material before disassembly. The delayed gammas have an energy of ~2 MeV. The opacity used in eqn (8) is defined by: $\mu = k/\rho$, where k is the linear absorption coefficient and ρ the mass density. Using Glasstone's Table 8.75 [27] and density values of 2.3, 7.9 and 11.3 g/cm^3 for concrete, iron and lead, respectively, one can construct a table (Table 2) for μ_γ.

Table 2. Gamma-ray mass absorption coefficient (cm^2/g) [27]

Energy (MeV)	H_2O	Concrete	Iron	Lead
2	0.049	0.050	0.042	0.046
5	0.030	0.031	0.032	0.044
10	0.022	0.026	0.029	0.054

The values in Table 2 should be contrasted with Glasstone's [27] choice (Section 8.79) of 0.023 cm^2/g as a value to use for most materials. For the estimates below we will use the "universal" value of 0.05 cm^2/g as appropriate for a 2 MeV gamma-ray.

5.2. X-rays

We will assume that the X-rays are emitted at a black-body temperature, T. Glasstone [27] (Section 7.8) states that most of the X-rays are emitted in the range of 0.1–100 Å (0.12–120 keV), the temperature being "several tens of millions of degrees Kelvin". Expressing T in units of keV, the black-body maximum is

$$\lambda_{max} = (2.5/T_{keV})\ \text{Å}$$

or

$$E_{max} = 5T_{keV}\ \text{keV}. \quad (24)$$

The ICARUS report [26] used $E_{max} = 120$ keV corresponding to $T = 24$ keV, but this appears too high. A temperature, $T = 2$ keV (2.3×10^7 K) for which $E_{max} = 10$ keV, seems more reasonable, at least for a fission device. In order to examine the sensitivity to the assumptions, Table 3 lists mass absorption data [30,31] for photon energies of 5, 10 and 25 keV; the latter value scaled from that at 10 keV according to $\mu_x \sim (1/E_{max})^3$. The choice of elements is discussed in Section 6 below. In principle, eqn (9) should be averaged over the Planck distribution; however, these data exist in tabular rather than analytical form and it was felt that this would have rendered the results less transparent.

Table 3. X-ray mass absorption coefficient (cm^2/g) [30,31]

	X-ray energy (keV)		
Element	5	10	25
Al	191	25.5	1.6
O	49	5.8	0.4
Mg	158	20.4	1.3
Si	244	33	2.1
Fe	138	176	11.3
Ca	637	96.5	6.2
S	353	49.6	3.2
Ni	180	215	13.8

Opacities for composite materials are estimated by summing over those of its constituents weighted according to their atomic percent, α_i:

$$\langle \mu \rangle = \sum_i \alpha_i \mu_i. \quad (25)$$

The X-ray absorption cross-sections ($Q = \mu_x A/N_0$, where A is the atomic weight and N_0 is the Avogadro's number) are three to four orders of magnitude greater than those for the neutrons, as will be discussed below, hence their penetration depth is correspondingly less.

Table 4. Neutron total cross-section (barns) [33]

	Neutron energy (MeV)	
Element	5	14
Al	2.4	1.7
O	1.0	1.5
Mg	2.0	1.65
Si	2.5	1.85
Fe	3.7	2.5
Ca	3.3	2.1
S	2.6	1.8
Ni	3.7	2.7

5.3. *Neutrons*

The principal reactions involved in the fusion of the hydrogen isotopes are [32]:

$$\begin{aligned} &D + D \rightarrow T(1.01\ \text{MeV}) + p(3.02\ \text{MeV}) \\ &\quad \rightarrow He^3(0.82\ \text{MeV}) + n(2.45\ \text{MeV}) \\ &D + T \rightarrow He^4 + n(14.1\ \text{MeV}) \\ &D + He^3 \rightarrow He^4 + p(14.7\ \text{MeV}) \\ &T + T \rightarrow He^4 + 2n + 11.3\ \text{MeV}. \end{aligned} \tag{26}$$

The two D–D reactions occur with approximately equal likelihood. The D–T reaction rate for temperatures between 10 and 30 keV is two orders of magnitude greater than that of the D–D and the other reactions and thus dominates in the range of interest. In what follows we will also ignore the reactions between the by-products. The neutrons, initially at 14 MeV, undergo collisions in the D–T fuel (assumed to be half consumed), in the case and other materials thus acquire an energy distribution or spectrum. Fortunately, the neutron cross-section is relatively insensitive both to the energy distribution and the material in our range of interest. For the fission neutron spectrum for slowing down in air at stp, Glasstone [27] (Fig. 8.96 and Section 8.104) uses a constant cross-section of $2b$ ($1b = 10^{-24}\ \text{cm}^2$). Assuming this applies to solid density matter ($N = 5 \times 10^{22}/\text{cm}^3$), this gives a mean-free-path of 10 cm. For the more energetic neutrons coming from the D–T reaction, taking a range of 5–14 MeV to partially take the spectrum into account, the cross-sections vary up and down by no more than a factor of two from the above, as can be seen in Table 4 [33]. Again the choice of elements is dictated by the materials of interest. For the estimates below we assume therefore, that all the neutrons are 14 MeV. The D–D neutrons contribute much less to the overall fusion energy due to their lower energy and to their reduced reaction rate and probability to occur.

Heating by neutrons requires a more detailed treatment than can be included in simple models. In particular, the elastic scattering of the neutrons by the ambient ions leads to recoil of the latter. These "knock-on" ions must be followed in-turn as they slow down and deposit their energy in the bulk of the material. The net result for the specific impulse may be intermediary between a constant absorption model and an exponential model. Therefore, both the constant absorption and exponential model results for the neutrons are contrasted in Section 7 below.

6. ATOMIC COMPOSITIONS OF ASTEROID MATERIALS' ANALOGS

The asteroid compositions described below and in Table 5, will be used to compare the effects of the various radiation sources. The models are based on meteorite analogs and are meant to be illustrative and are tentative pending further data [34,35]. The chondrite groups [36], are subdivided into non-volatile-free (NVF) and volatile (S, O, C, H)-free (VF) in order to account for the possibility of outgassing of a surface layer during the first of several bursts.

(1) Iron–nickel
Composition: 90% Fe, 7-8% Ni (atomic %)
Density: 7.9 g/cm^3
(2) Enstatite
Composition: see Table 5
Density: 4 g/cm^3
(3) Ordinary chondrite
Composition: see Table 5
Density: 3.4 g/cm^3
(4) Carbonaceous chondrites
Composition: see Table 5
Density: 2.1 g/cm^3

Öpik's [28] values for the vaporization energies of iron and stony meteorites are 8.26×10^{10} and 8.08×10^{10} ergs/g, respectively, while Bronshten [37] uses the value of $\epsilon_v = 8.0 \times 10^{10}$ ergs/g for all meteorites. The latter value will be adopted here as well.

Table 5. Composition (atomic %) of chondrite groups [36]

	Enstatite		Ordinary		Carbonaceous	
Element	NVF	VF	NVF	VF	NVF	VF
Si	16.44	34.7	16.0	37.3	13.9	32.0
Al	0.81	1.7	1.2	2.8	1.2	2.9
Fe	16.44	34.6	9.4	22.0	11.39	26.3
Mg	12.13	25.6	14.9	35.0	15.1	34.9
Ca	0.81	1.7	0.8	1.7	0.99	2.3
Ni	0.81	1.7	0.5	1.2	0.74	1.7
S	5.12	—	1.7	—	1.48	—
O	47.44	—	55.88	—	55.2	—

NVF = non-volatile free; VF = volatile free.

Table 6. 10 keV X-ray and 14 MeV neutron mass absorption coefficients (cm^2/g)

	$\langle\mu_X\rangle$	$\langle\mu_N\rangle$
Enstatite NVF	44.9	4.8×10^{-2}
Enstatite VF	83.5	3.6×10^{-2}
Ordinary NVF	30.6	5.1×10^{-2}
Ordinary VF	63.4	3.8×10^{-2}
Carbonaceous NVF	34.6	5.0×10^{-2}
Carbonaceous VF	70.8	3.8×10^{-2}
Fe/Ni (90%/10%)	180	2.8×10^{-2}

NVF = non-volatile free; VF = volatile free.

7. RESULTS

The above information can now be combined into estimates of the yields required for given velocity increments, densities and diameter. First consider the gamma-ray contribution. The non-dimensional parameter F_0^*, in units already defined, with the value of ϵ_γ given above, and on using eqns (11) and (12), is given by:

$$F_0^* = (16.66)\frac{\mu\eta\Delta\Omega Y(\mathrm{MT})}{D^2}. \tag{27}$$

Using the parameters for gamma-rays, $F_0^* \approx (0.008)Y(\mathrm{MT})/D^2$. Thus gamma-rays, especially for large NEOs, will not make a significant contribution until around the 1000 MT range.

Equation (21) can be simplified by defining,

$$y = m^*\Delta V^*/2\sqrt{2}$$

$$\phi = (F_0^* - 1)^{1/2}$$

so that

$$y = \phi - \tan^{-1}(\phi). \tag{28}$$

Here y is, apart from the numerical factors, the non-dimensional momentum transferred to the NEO, while $\phi^2 + 1$ is the non-dimensional fluence.

Expressed in terms of the physical quantities,

$$y = \rho\mu D\Delta V/2\sqrt{2\epsilon_\gamma} = \rho\mu D\Delta V/48. \tag{29}$$

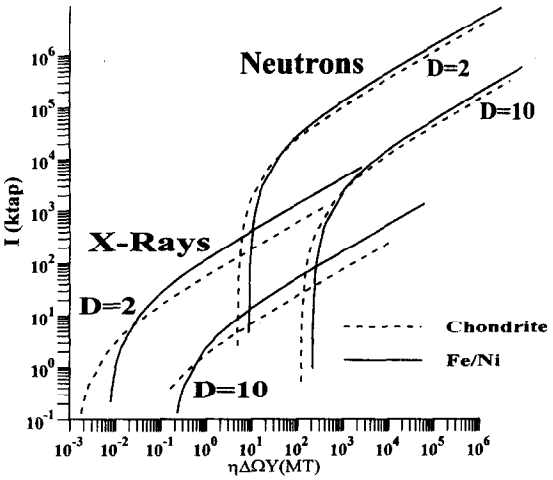

Fig. 3. Specific impulse (ktaps) vs the yield parameter $[\eta\Delta\Omega Y(\mathrm{MT})]$ produced by 10 keV X-ray and 14 MeV absorption for $D = 2$ km and $D = 10$ km chondrite and Fe/Ni asteroid models.

Again we have used the value of ϵ_γ given at the end of Section 6.

The X-ray and neutron opacities, averaged over the atomic percents, are listed in Table 6. Representative values for the X-ray opacities are 35 cm^2/g for non-volatile free chrondites, about twice that value for the volatile-free material, and 180 cm^2/g for Fe/Ni NEOs. The corresponding neutron opacities are 0.05 and 0.028 cm^2/g for all chrondites and iron/nickel NEOs, respectively. From eqn (29) the density and opacity enter as a product, so that the value of y for neutron interactions is approximately the same for the chondrites and Fe/Ni NEOs.

Since y is proportional to the opacity, the low opacities for neutrons result in their values for y falling in the region where the full expression [eqn (28)] must be used. The X-ray opacities are sufficiently high that their values for the non-

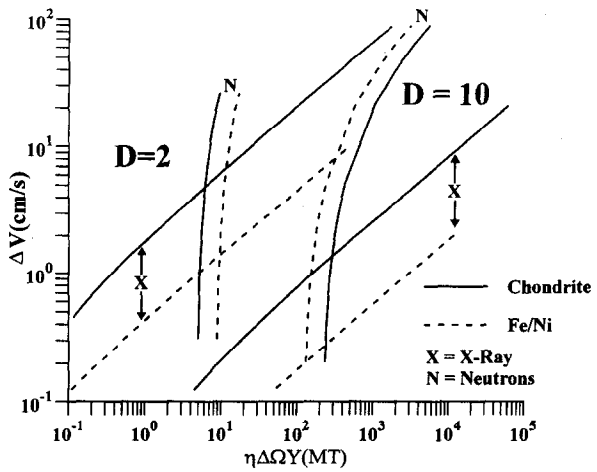

Fig. 2. Velocity imparted by 10 keV X-ray and 14 MeV neutron absorption vs the yield parameter $[\eta\Delta\Omega Y(\mathrm{MT})]$ for $D = 2$ km and $D = 10$ km chondrite and Fe/Ni asteroid models.

dimensional momentum parameter fall in the asymptotic region. It is useful to present this information in its dimensional form. The desired velocity increment, ΔV (cm/s), is plotted in Fig. 2 versus the quantity $\eta Y(\mathrm{MJ})\Delta\Omega$, known as the yield parameter, for an X-ray and neutron radiation of 2 and 10 km diameter chondrite and Fe/Ni asteroids. Figure 3 shows results for the specific impulse for the same parameters.

8. DISCUSSION AND CONCLUSION

The trends seen in Figs 2 and 3 are due to the large differences in the opacities for X-ray and neutron absorption. This behavior can be explained by considering eqn (28), for X-rays $y \gg 1$ and $\phi \approx y$, whereas for neutron absorption $y \ll 1$ and $\phi \approx (3y)^{1/3}$. In this application, X-ray absorption in the exponential model can be approximated by its asymptotic limit whereas neutron effects cannot. In the asymptotic limit both the velocity change and the specific impulse are inversely proportional to the inverse square root of the opacity, proportional to the square root of the flux, and independent of the heat of vaporization. The effect of neutron irradiation requires use of the full expression and therefore exhibits the steep cut-off behavior seen in the figures, which occurs when the non-dimensional flux parameter $F_0^* \approx 1$. The exponential absorption model thus gives, for X-ray and neutron absorption respectively:

$$\begin{aligned} Y(\mathrm{MT})\Delta\Omega/D^2 &\approx 0.06(\rho D\Delta V/48)^2\mu_x/\mu_x \\ &\approx 1.2[1+(3y)^{2/3}]/\eta_N \\ &\approx 0.06[1+4y^2]/\eta_N. \end{aligned} \tag{30}$$

The last line of eqn (30) is the result for the constant absorption model for neutron absorption.

As discussed in Section 1, the contribution to ΔV from the debris for asteroid diameters greater than 1 km can be neglected to first approximation as compared to that from X-rays and neutrons.

For the NEO materials considered, the exponential model indicates that when $D\Delta V = 1$, $Y(\mathrm{MT})\Delta\Omega/D(\mathrm{km})^2$ is smaller for X-rays than for neutrons, while for $D\Delta V = 10$, the reverse is true with neutrons having a significant advantage over X-rays in this range. As shown in Figs 2 and 3, neutrons are more effective than X-rays in imparting velocity changes to large Fe/Ni objects. The greater penetration of the neutrons implies that more mass is ablated and hence larger yields are required than for X-ray ablation, however, for large objects ($\geqslant 10$ km), neutrons would appear to be required for velocity increments in excess of a few cm/s. The exponential model, for a given diameter and $D\Delta V$ product, requires a substantially higher yield than that for constant absorption when applied to ablation by neutrons.

From eqns (23) and (27), the maximum impulse coupling coefficient occurs for $F_0^*/16.6 = 0.386$, $y = 1.166$. For neutron interactions, this implies $D\Delta V \approx 280$, while for X-ray ablation of VF chondrites, NVF chondrites and Fe/Ni, one has $D\Delta V \approx 0.4$, 0.2, and 0.04, respectively.

Due to the difference in velocities there will be a tendency for the X-rays to "fire polish" the asteroid's surface before arrival of the neutrons. Scattering of the neutrons in this "atmosphere" has not been considered in this paper, though it is not expected to be important due to the short time involved.

The above conclusions depend critically on the assumed radiation spectrum and the values used for the opacities as well as the very simple model. Hence, the results should be taken as indicative pending more elaborate estimates. A first-order improvement, still using the simple model, would be to use radiative opacities averaged over the Planck distribution. One would then substitute, for the opacities used here, those derived by suitably averaging them using the Rosseland mean. The Rosseland opacity is given by [38]:

$$\mu_R = (15/4\pi^4)\int_0^{\infty} \mu \frac{u^4 e^{-u}}{(1-e^{-u})^3}\,du$$
$$u = E/\Theta \tag{31}$$

where E is the X-ray photon energy and Θ the black body temperature. Thus in Section 3 one would replace μ by μ_R wherever it appears. If we further assume that $\mu \sim 1/E^m$, then it is easily shown that $\mu_R \sim 1/\Theta^m$ and hence, using eqn (16), the specific impulse should vary as $I \sim \Theta^{m/2}$. For a hydrogenic plasma $m = 3.5$, while for cold matter $m = 3$. Integrating over all the absorption lines of a given material can lead to a different value of m. For example, from Fig. 11 of Shafer *et al.* [20], in the large fluence limit, $m \cong 2.0$.

Confirmation from a subsidiary calculation as to the range of validity of the exponential model in treating the neutron effects is also necessary since the sensitivity of the neutron results in the simple model used herein implies that more elaborate calculations are desirable. In inertial confinement fusion, the thermonuclear energy comes from a highly compressed and heated target consisting of a DT fuel surrounded by a container. Magelssen and Moses [39] have studied, in the context of fusion reactor designs, the X-ray and neutron spectra emitted from such targets where the shell was a high-Z material (Hg). The spectra they find are consistent with those we have used. Our results are also consistent with the work of Shafer *et al.* [20], both for X-rays and for neutrons. Their neutron results also include two points derived from a hydro-code calculation. In a recent paper, a team at the Ecole Polytechnique [40] have performed experiments on the impulse imparted to a metallic target by soft X-rays. Their results confirm the general trends of the model discussed above as applied to X-rays. However, more experiments along these lines are needed.

Finally, recent ground-based radar observations indicate that some near-Earth asteroids are far from spherical [41], a complication that will have to be taken into account in future simulations.

The potentially important case of nuclear radiation interaction with comets has not been treated explicitly in this paper, but may be approximated by using the materials properties of carbonaceous chondrites, which some believe are similar in composition to dormant or volatile depleted comets. This will be discussed elsewhere using a newly developed model for comets [42].

Acknowledgements—The authors are grateful to Paul Sherard and J. C. Remo for their help with the figures. The authors also wish to thank the reviewer for his very helpful comments and suggestions.

REFERENCES

1. E. F. Helin and E. M. Shoemaker, Palomar planet-crossing asteroid survey 1973–1978. *Icarus* **40,** 321–328 (1979).
2. E. M. Shoemaker, R. F. Wolfe and C. S. Shoemaker, Asteroid and comet flux in the neighborhood of the Earth. *Geol. Soc. Am. Spec. Pap.* **247,** 155–170 (1990).
3. D. Rabinowitz, E. Bowell, G. Shoemaker and K. Muinonen, The population of Earth-crossing asteroids. In *Hazards Due to Meteorites and Comets* (Edited by T. Gehrels), pp. 285–312. University of Arizona Press, Tucson, AZ (1994).
4. R. P. Binzel, S. Xu, S. J. Bus and E. Bowell, Origins for the near-Earth asteroids. *Science* **257,** 779–782 (1992).
5. E. M. Shoemaker and C. S. Shoemaker, The crash of P/Shoemaker–Levy 9 into Jupiter and its implication for comet bombardment on Earth. In *New Developments Regarding the KT Event and Other Catastrophes in Earth History*. LPI Contribution No. 825, p. 113. Lunar and Planetary Institute, Houston, TX (1994).
6. L. W. Alvarez, W. Alvarez, F. Asaro and H. V. Michel, Extraterrestrial cause for the cretaceous–tertiary extinction. *Science* **208,** (1980).
7. J. K. Beatty and S. J. Goldman, The great crash of 1994: a first report. *Sky Telesc.* **88,** 18–23 (1994).
8. E. M. Shoemaker, NASA Workshop, *Collisions of Asteroids and Comets with Earth: Physical and Human Consequences*, Snowmass, CO, 13–16 July (1981). Called "Snowmass report" in the text.
9. G. H. Canavan, J. C. Solem and J. D. G. Rather (eds), *Proceedings of the Near Earth Object Interception Workshop*, 14–16 January. Los Alamos National Laboratory, Los Alamos NM, LA-12476-C (1992).
10. T. Gehrels (ed.), *Hazards Due to Meteorites and Comets*. University of Arizona Press, Tucson AZ (1994).
11. D. Morrison, The Spaceguard Survey: Report of the NASA International Near-Object Detection Workshop, 10 January, 1992, Jet Propulsion Laboratory/California Institute of Technology, Pasadena, CA (1992).
12. New developments regarding the KT event and other catastrophes in Earth history, LPI Contribution No. 825, p. 138. Lunar and Planetary Institute, Houston, TX (1994).
13. J. L. Remo (ed.), *Proceedings of the United Nations Conference on Near-Earth Objects*. In preparation (1996).
14. C. R. Chapman and D. Morrison, Impacts on the Earth by asteroids and comets: assessing the hazard. *Nature* **367,** 33–40 (1994).
15. T. Beardsley, Big bang. *Scient. Am.* **265** (1991).
16. A. C. Levasseur-Regourd, 26 Septembre 2000: la Collision? *Sci. Avenir* **548,** 49 (1992).
17. T. J. Ahrens and A. W. Harris, Deflection and fragmentation of near-Earth asteroids. *Nature* **360,** 429–433 (1992).
18. T. J. Ahrens and A. W. Harris, Deflection and fragmentation of near-Earth asteroids. In *Hazards Due to Meteorites and Comets* (Edited by T. Gehrels), pp. 897–927. University of Arizona Press, Tucson, AZ (1994).
19. J. L. Remo and P. M. Sforza, Subsurface momentum coupling momentum analysis for near-Earth-object orbital management. *Acta Astronautica* **35,** 27–33 (1995).
20. B. P. Shafer, M. D. Garcia, R. A. Managan, J. L. Remo, C. E. Rosenkilde, R. J. Scammon, C. M. Snell and R. F. Stellingwerf, The coupling of energy to asteroids and comets. In *Hazards Due to Comets and Asteroids* (Edited by T. Gehrels), pp. 955–1012. Tucson, Arizona, AZ (1994).
21. R. A. Hyde, Cosmic bombardment. Lawrence Livermore National Laboratory Report UCID-20062 (1984).
22. P. Hammerling and J. L. Remo, NEO interaction with X-ray and neutron radiation. In *Proceedings of the Near Earth Object Interception Workshop* (Edited by G. H. Canavan, J. C. Solem and J. D. Rather), pp. 186–193. Los Alamos National Laboratory, Los Alamos, NM, LA-12476-C (1992).
23. N. Bloembergen (Chairman), Report to the American Physical Society by the Study Group on Science and Technology of Directed Energy Weapons. *Rev. Mod. Phys.* **59** (1987). Called "APS report" in the text.
24. R. J. Lawrence, An effective properties model for pulsed radiation interactions. Sandia National Laboratories Report, SAND88-0245 (1988).
25. R. J. Lawrence, The equivalence of simple models for radiation-induced impulse. Sandia National Laboratory Report, SAND 91-1171C9 (1991).
26. L. A. Kleinman (Ed.), Project ICARUS. MIT Report 13, MIT Press, Cambridge (1968). Called "ICARUS report" in the text.
27. S. Glasstone (Ed.), *The Effects of Nuclear Weapons*. U.S. AEC (1962). Called "Glasstone" in the text.
28. E. J. Öpik, *Physics of Meteor Flight in the Atmosphere*. Interscience, New York (1958).
29. C. R. Phipps Jr, T. P. Turner, R. F. Hanson, G. W. York, W. Z. Osborne, G. K. Anderson, X. F. Corlis, L. C. Haynes, H. S. Steele, K. C. Spicochi and T. R. King, Impulse coupling to targets in vacuum by KrF, HF, and CO_2 single-pulse lasers. *J. Appl. Phys.* **64,** 1083–1096 (1988).
30. B. L. Henke, P. Lee, T. J. Tanaka, R. L. Shimabukero and B. K. Fujikawa, *At. Data Nucl. Data Tables* **27,** 1 (1982).
31. D. Vaughan, *X-Ray Data Booklet*. Center for X-Ray Optics, Lawrence Berkeley, Laboratory, Berkeley, CA (1986).
32. S. Glasstone and R. Lovberg, *Controlled Thermonuclear Reactions*. Van Nostrand, Princeton, NJ (1960).
33. V. McLane, C. L. Dunford and P. F. Rose, *Neutron Cross-sections*. Academic Press, Boston, MA (1988).
34. J. L. Remo, Asteroid/meteorite analogs and materials properties. In *Proceedings of the Near Earth Object Interception Workshop* (Edited by G. H. Canavan, J. C. Solem and J. D. G. Rather), pp. 163–174. Los Alamos National Laboratory, Los Alamos, NM, LA-12476-C (1992).
35. J. L. Remo, Classifying and modeling material properties and interactions. In *Hazards Due to Meteorites and Comets* (Edited by T. Gehrels), pp. 551–596. University of Arizona Press, Tucson, AZ (1994).
36. J. T. Dodd, *Meteorites*. Cambridge University Press, Cambridge, U.K. (1981).

37. V. A. Bronshten, *Physics of Meteoric Phenomena*. Reidel, Dordrecht (1983).
38. Ya. B. Zeldovich and Yu. P. Raizer, *Physics of Shock Waves and High-temperature Phenomena* (Edited by W. D. Hayes and R. P. Probstein). Academic Press, New York (1966).
39. G. R. Magelssen and G. A. Moses, Pellet X-ray spectra for laser fusion reactor designs. *Nucl. Fusion* **19**, 301–311 (1979).
40. J. C. Gautier, C. Chenais-Popovics, F. Puech, P. Renaudin and L. Visconti, Impulse generated by a laser-produced X-ray source on a metallic layer. In *Applications of Laser Plasma Radiation* (Edited by M. C. Richardson), pp. 220–226. SPIE **2015** (1994).
41. S. J. Ostro, K. D. Rosema, R. S. Hudson, R. F. Jurgens, J. D. Giorgini, R. Winkler, D. K. Yeomans, D. Choate, R. Rose, M. A. Slade, S. D. Howard and D. L. Mitchell, Extreme elongation of asteroid 1620 geographos from radar images. *Nature* **375**, 474–476 (1995).
42. J. M. Greenberg and J. L. Remo, A current working model of a comet nucleus and implications for NEO interactions. *Hazards Due to Meteorites and Comets* (Edited by T. Gehrels), pp. 635–647. University of Arizona Press, Tucson, AZ (1994).